Plasmon damping and response function in doped C_{60} compounds

1996 J. Phys.: Condens. Matter 8 4001

(http://iopscience.iop.org/0953-8984/8/22/005)

J. Phys.: Condens. Matter **8** (1996) 4001–4016. Printed in the UK

Plasmon damping and response function in doped C_{60} compounds

A I Liechtenstein†, O Gunnarsson†, M Knupfer‡, J Fink‡ and J F Armbruster§

† Max-Planck-Institut für Festkörperforschung, D-70506 Stuttgart, Germany
‡ Institut für Festkörperforschung, IFW Dresden, Postfach 270016, D-01171 Dresden, Germany
§ Forschungszentrum Karlsruhe, Institut für Nukleare Festkörperphysik, Postfach 3640, D-76021 Karlsruhe, Germany

Received 23 February 1996

Abstract. We present experimental and theoretical results for the broadening of the 0.5 eV charge carrier plasmon in A_3C_{60} (A = K, Rb) compounds. The experimental width (0.5 eV) is very large and comparable to the plasmon energy. We have performed RPA calculations for a three-band model of orientationally disordered C_{60} molecules. We show that it is unlikely that the width can be caused by the disorder or by a decay in single electron–hole pair excitations. Instead we have studied the decay in an electron–hole pair dressed by phonon excitations. We have calculated the response function, using Green's functions dressed by the self-energy due to the electron–phonon interaction. Vertex corrections are included to satisfy the Ward identity. We show that this leads to a width of the plasmon which is comparable to its energy, in agreement with experiment.

1. Introduction

The doped C_{60} compounds, K_3C_{60} and Rb_3C_{60} have a plasmon with an energy of about 0.5 eV [1]. This corresponds to a collective oscillation of the electrons in the partly filled t_{1u} band donated by the alkali atoms, for which the remaining 240 electrons essentially only contribute a background dielectric function. Here we present measurements for single-phase K_3C_{60}, showing that the width of the plasmon is about 0.5 eV, comparable to the energy of the plasmon. The origin of this width is unclear. Normally, a large width is due to the decay of the plasmon in electron–hole pairs. Band structure calculations, however, find the width of the t_{1u} band to be about $\frac{1}{2}$ eV [2]. Even if this may allow for some decay of the plasmon into electron–hole pairs, one would then expect a strongly non-symmetric line shape, since there are few or no electron–hole pairs available at the upper flank of the plasmon at energies of the order $0.5 + 0.5/2 = 0.75$ eV, unless band structure calculations greatly underestimate the width of the band. In that case it would, however, be hard to understand why the band structure calculations give a reasonable density of states [3]. In free-electron-like metals, disorder can cause a broadening of the plasmon at small values of q, since the plasmon can decay in electron–hole pairs of the appropriate energy, which in the absence of disorder would have had too large momenta. Although doped C_{60} compounds have orientational disorder, with each molecule taking one of two possible orientations essentially randomly [4], this broadening mechanism is not possible if the estimates of the band width are roughly correct, since there are then not enough electron–hole pairs available at any momentum.

0953-8984/96/224001+16$19.50

It therefore seems likely that the width of the plasmon is caused by a mechanism other than a simple decay into one electron–hole pair. The disorder could influence the apparent width in a different way. In the system without disorder, the plasmon may have a dispersion as a function of the momentum transfer q. As the disorder is introduced, momentum conservation is violated and plasmons with different q vectors may couple. This could possibly show up as a large broadening of an apparently dispersionless plasmon. To test this we have performed an RPA calculation for a system with disorder, including the three t_{1u} levels for each C_{60} molecule. These calculations give much too small a broadening to explain the experimental width. The strong Coulomb interaction in C_{60} could cause the decay in multiple electron–hole pairs. It could also cause the decay into more complicated states, where the Coulomb energy is larger in the final state, which would take up some of the plasmon energy. While mechanisms of this type may play a role for the plasmon broadening, we have here studied a different mechanism.

The C_{60} compounds are known to have a strong electron–phonon interaction [5]. The plasmon could therefore decay into an electron–hole pair under the emission of one or several phonon(s). Some of the plasmon energy would then be taken up by the phonon(s). We find that the electron–phonon interaction indeed leads to a large broadening of the plasmon. Due to the finite band width, the electronic states at the bottom and at the top of the band are pushed out of the band by the electron–phonon interaction, thereby increasing the quasiparticle band width substantially. This seems to be the most important effect of the electron–phonon interaction.

In this paper we study a one-band, tight-binding model with a coupling to an Einstein phonon on each molecule, describing the intramolecular phonons. To describe the plasmon we have to calculate the dielectric function as a function of q and ω, since the plasmon shows up as a peak in $-\mathrm{Im}\ \epsilon^{-1}$, and the width of this peak gives the broadening.

The polarizability is expressed in terms of the electron Green's function, dressed by the self-energy due to the electron–phonon interaction. To satisfy the Ward identity [6], resulting from charge and current conservation, it is important to add vertex corrections in a consistent way. We have included mixed ladder diagrams, where the rungs are electron and phonon lines, with the phonon lines being dressed phonon Green's functions. The vertex corrections have earlier been treated by Holstein [7], who studied these corrections in the context of the resistivity and the phonon drag effect. Holstein considered the case when the Fermi energy is much larger than the frequencies of the phonons and the external field. Here we consider the response function for the case when the Fermi energy, the phonon energy and the frequency of the external field are comparable, which leads to qualitatively new features.

In section 2 we present the RPA calculations for a three-band model of the disordered system. In section 3 we describe the formalism for including the electron–phonon interaction, and in section 4 the model and the details of the calculation. In section 5 we present experimental results and results for the dielectric function and the plasmon broadening with the electron–phonon coupling included.

2. Disordered system

We first consider a disordered system, to see if disorder can explain the broadening of the plasmons.

We consider a large supercell of N disordered C_{60} molecules. A certain tendency to an 'anti-ferromagnetic' ordering of the molecules, with neighbouring molecules having the different orientation, has been predicted theoretically [8, 9], and observed

experimentally [10]. Here we neglect this tendency to local correlation and consider molecules which randomly take one of the two preferred orientations [4]. For each molecule we include the three t_{1u} orbitals. The remaining C_{60} molecular orbitals contribute a background dielectric function, which only modifies the plasmon energy and dispersion [11]. Within this model the plasmon has a substantial negative dispersion for the ordered system [11], and we are able to test the effects of coupling plasmons which have different energies for different values of q. We thus consider the one-particle Hamiltonian

$$H = \sum_i \sum_{L=1}^{3} \sum_\sigma \varepsilon_0 n_{iL\sigma} + \sum_{iLjL'\sigma} \left[t(iL, jL')\psi^\dagger_{iL\sigma}\psi_{jL'\sigma} + \mathrm{HC} \right] \tag{1}$$

where i labels the molecules and L labels the three t_{1u} orbitals. The hopping integrals $t(iL, jL')$ are chosen to take the orientational disorder into account, i.e., they depend on the orientations of the molecules involved [9]. The supercell is periodically repeated. The Coulomb integrals between the t_{1u} orbitals are calculated by using a representation of the t_{1u} orbitals in terms of 'radial' 2p orbitals located on the carbon atoms in a C_{60} molecule and pointing radially out from the the centre of the molecule [8]. Based on atomic calculations, we put the Coulomb interaction between two electrons on the same atom equal to 12 eV [12]. The Coulomb interaction between two electrons on different atoms is assumed to be e^2/r, where r is the separation between the two atoms. All other Coulomb integrals, involving orbitals on three or four different atoms, are neglected [12].

In the RPA, the irreducible polarizability for the frequency ω is given by

$$P_0(\boldsymbol{r}, \boldsymbol{r}', \omega) = 2 \sum_{\boldsymbol{k}n\boldsymbol{k}'n'} \frac{\psi_{\boldsymbol{k}n}(\boldsymbol{r})\psi^*_{\boldsymbol{k}n}(\boldsymbol{r}')\psi^*_{\boldsymbol{k}'n'}(\boldsymbol{r})\psi_{\boldsymbol{k}'n'}(\boldsymbol{r}')}{\varepsilon(\boldsymbol{k}n) - \varepsilon(\boldsymbol{k}'n') - \omega} \times \left[f(\boldsymbol{k}n) - f(\boldsymbol{k}'n') \right] \tag{2}$$

where $\psi_{\boldsymbol{k}n}(\boldsymbol{r})$ is the wavefunction for a state $\boldsymbol{k}n$ with the energy $\varepsilon(\boldsymbol{k}n)$. Here $\boldsymbol{k}$ refers to a wavevector in the small Brillouin zone corresponding to the supercell and n runs over $3N$ states. $f(\boldsymbol{k}n)$ is the Fermi function and a factor two comes from summation over spin. The states $\psi_{\boldsymbol{k}n}(\boldsymbol{r})$ are expressed as

$$\psi_{\boldsymbol{k}n}(\boldsymbol{r}) = \frac{1}{\sqrt{M}} \sum_{iL\alpha} \mathrm{e}^{\mathrm{i}\boldsymbol{k}\cdot\boldsymbol{R}_\alpha} c_{iL}(\boldsymbol{k})\phi_L(\boldsymbol{r} - \boldsymbol{R}_i - \boldsymbol{R}_\alpha) \tag{3}$$

where $\boldsymbol{R}_i$ gives the positions of the C_{60} molecules in the supercell and $\boldsymbol{R}_\alpha$ the positions of the M supercells, and $\phi_L(\boldsymbol{r})$ describes the three t_{1u} orbitals. We use products of t_{1u} orbitals as basis states for the polarizability

$$\Phi_{\boldsymbol{q}iLL'}(\boldsymbol{r}) \equiv \Phi_{\boldsymbol{q}\nu}(\boldsymbol{r}) = \frac{1}{\sqrt{M}} \sum_\alpha \mathrm{e}^{\mathrm{i}\boldsymbol{q}\cdot\boldsymbol{R}_\alpha} \phi_L(\boldsymbol{r} - \boldsymbol{R}_i - \boldsymbol{R}_\alpha)\phi_{L'}(\boldsymbol{r} - \boldsymbol{R}_i - \boldsymbol{R}_\alpha) \tag{4}$$

where we have used $\nu \equiv iLL'$ as a combined index and we assume that the overlap between t_{1u} orbitals on different molecules can be neglected. We then obtain

$$P_0(\boldsymbol{r}, \boldsymbol{r}', \omega) = \sum_{\boldsymbol{q}} \sum_{iLL'} \sum_{jL_1L_2} \Phi^*_{\boldsymbol{q}iLL'}(\boldsymbol{r}) \times \tilde{P}_0(iLL', jL_1L_2, \boldsymbol{q}, \omega)\Phi_{\boldsymbol{q}jL_1L_2}(\boldsymbol{r}) \tag{5}$$

where

$$\tilde{P}_0(iLL', jL_1L_2, \boldsymbol{q}, \omega) = 2\sum_{\boldsymbol{k}nn'} \frac{c_{\boldsymbol{k}iL}(n)c^*_{iL'}(\boldsymbol{k}+\boldsymbol{q}n')c^*_{jL_1}(\boldsymbol{k}n)c_{jL_2}(\boldsymbol{k}+\boldsymbol{q}n')}{\varepsilon(\boldsymbol{k}n)-\varepsilon(\boldsymbol{k}+\boldsymbol{q}n')-\omega} \times [f(\boldsymbol{k}n)-f(\boldsymbol{k}+\boldsymbol{q}n')]. \tag{6}$$

To avoid linear dependencies we introduce the restriction $L \leqslant L'$ in $\Phi_{\boldsymbol{q}iLL'}(\boldsymbol{r})$. In this way we have expressed the irreducible polarizability in terms of matrices with the dimension $6N$, where N is the number of molecules in the cluster. In the limit when the supercell becomes very large, the dependence of $\varepsilon(\boldsymbol{k}n)$ on $\boldsymbol{k}$ becomes very weak. Here we neglect this dependence and replace the sum over $\boldsymbol{k}$ by the results for $\boldsymbol{k}=0$. It is, however, essential to calculate the coefficients $c_{iLL'}(\boldsymbol{k}+\boldsymbol{q})$ for the proper value of $\boldsymbol{q}$ to obtain appropriate phase factors in the polarizability.

We now consider the screening of an external potential

$$V^{ext}(\boldsymbol{r},t) = V^{ext}(\boldsymbol{r},\omega)\mathrm{e}^{-\mathrm{i}\omega t} = V^{ext}(\boldsymbol{q},\omega)\mathrm{e}^{-\mathrm{i}\omega t}\mathrm{e}^{\mathrm{i}\boldsymbol{q}\cdot\boldsymbol{r}}/\sqrt{M\Omega} \tag{7}$$

where Ω is the volume of the unit cell and M is the number of unit cells. The screened potential, $V^{scr}(\boldsymbol{r},\omega)$, satisfies the equation

$$V^{scr}(\boldsymbol{r},\omega) = V^{ext}(\boldsymbol{r},\omega)/\epsilon_0 + + \int \mathrm{d}^3r' \int \mathrm{d}^3r'' \frac{v(\boldsymbol{r}-\boldsymbol{r}')}{\epsilon_0} P^0(\boldsymbol{r}',\boldsymbol{r}'',\omega)V^{scr}(\boldsymbol{r}'',\omega) \tag{8}$$

where $v(\boldsymbol{r}-\boldsymbol{r}')$ is the unscreened Coulomb interaction and ϵ_0 is the dielectric function due to the interband transitions not included explicitly in the model. This equation describes how the screened potential induces a charge density P^0V^{scr} and an induced potential vP^0V^{scr}. To solve for V^{scr}, we introduce

$$\tilde{V}^{scr}_{iLL'}(\boldsymbol{q},\omega) = \int \mathrm{d}^3r \Phi_{\boldsymbol{q}iLL'}(\boldsymbol{r})V^{scr}(\boldsymbol{r},\omega) \tag{9}$$

together with a similar definition for $\tilde{V}^{ext}$. We then find

$$\tilde{V}^{scr}_{\nu}(\boldsymbol{q},\omega) = \tilde{V}^{ext}_{\nu}(\boldsymbol{q},\omega)/\epsilon + \sum_{\mu,\nu'} \frac{\tilde{v}_{\nu\mu}(\boldsymbol{q})}{\epsilon} \tilde{P}^0_{\mu\nu'}(\mathrm{i}\boldsymbol{q},\omega)\tilde{V}^{scr}_{\nu'}(\boldsymbol{q},\omega) \tag{10}$$

where $\tilde{v}_{\nu,\mu}(\boldsymbol{q})$ is a matrix element between two functions $\Phi_{\boldsymbol{q}\nu}$ and $\Phi^*_{\boldsymbol{q}\mu}$ of the Coulomb interaction. We then find the dielectric matrix

$$\tilde{\epsilon}^{-1}_{\nu\mu}(\boldsymbol{q},\omega) = \frac{\tilde{V}^{scr}_{\nu}}{\tilde{V}^{ext}_{\mu}} = [(\epsilon_0 - \tilde{v}\tilde{P}^0)^{-1}]_{\nu\mu}. \tag{11}$$

Inelastic electron scattering measures a quantity which is related to

$$\mathrm{Im}\ \epsilon^{-1}(\boldsymbol{q},\omega) = \sum_{iLL'}\sum_{jL_1L_2} \mathrm{e}^{\mathrm{i}\boldsymbol{q}\cdot(\boldsymbol{R}_i-\boldsymbol{R}_j)}\langle L|\mathrm{e}^{\mathrm{i}\boldsymbol{q}\cdot\boldsymbol{r}}|L'\rangle \times [(\epsilon - \tilde{v}\tilde{P}^0)^{-1}]_{iLL',jL_1L_2}\langle L_1|\mathrm{e}^{-\mathrm{i}\boldsymbol{q}\cdot\boldsymbol{r}}|L_2\rangle \tag{12}$$

where $\langle L|\mathrm{e}^{\mathrm{i}\boldsymbol{q}\cdot\boldsymbol{r}}|L'\rangle$ is a matrix element of $\mathrm{e}^{\mathrm{i}\boldsymbol{q}\cdot\boldsymbol{r}}$ between two t_{1u} orbitals.

We have performed calculations for a model with 32 molecules in the supercell. As discussed elsewhere [11], if the interband transitions are allowed to contribute the

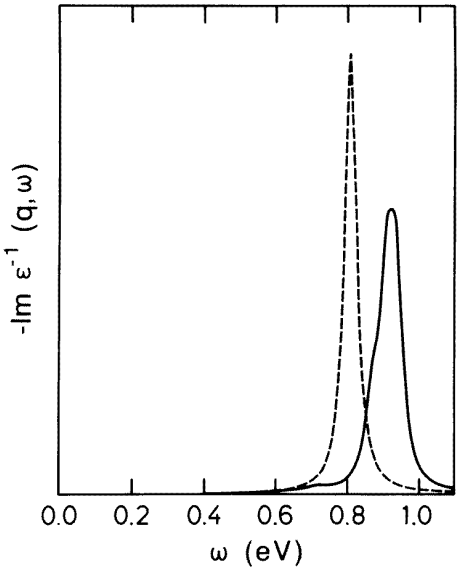

(*a*)

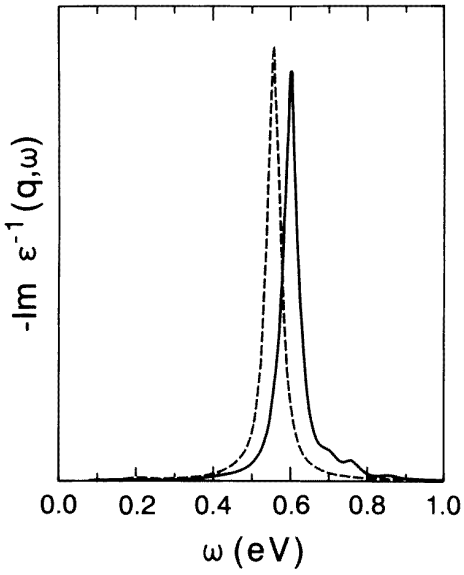

(*b*)

Figure 1. $-\mathrm{Im}\ \epsilon^{-1}(\boldsymbol{q},\omega)$ for $\boldsymbol{q} = (0.25, 0.0, 0.0)$ Å^{-1} (a) and $\boldsymbol{q} = (0.45, 0.0, 0.0)$ Å^{-1} (b) as a function of ω. A broadening with the full-width half-maximum 0.04 eV has been introduced. The full line shows the result for a disordered cluster and the dashed line for an ordered cluster.

experimentally observed dielectric constant, the calculated t_{1u} band width has to be multiplied by about a factor 0.6 to give the observed plasmon energy. This large reduction may be due to the RPA approximation and may suggest that many-body effects are important, or it could be due to the model not being sufficiently realistic. Here we first use this band

width but neglect the dielectric function from the interband transitions ($\epsilon = 1$). For the ordered infinite system, the plasmon energy is then 1.06 eV for $q = 0$ and about 0.6 eV at the Brillouin zone boundaries [11], which for the (100) direction occurs for $|\boldsymbol{q}| = 0.44$ Å^{-1}.

In figure 1(a) we show results for $\boldsymbol{q} = 2\pi/a(0.25, 0.0, 0.0)$ for both an ordered and a disordered cluster. For the ordered cluster the plasmon is narrow and the width is due to the artificial broadening (0.04 eV) introduced in the calculation. The introduction of disorder leads to additional structures, and a tail towards lower energies. The width (~ 0.1 eV) is, however, much smaller than what is seen experimentally (0.5 eV). In figure 1(b) we show results for $\boldsymbol{q} = (0.45, 0, 0)$ Å^{-1}. For this $\boldsymbol{q}$ vector there is little extra broadening due to the disorder, although there is a weak tail towards higher energies.

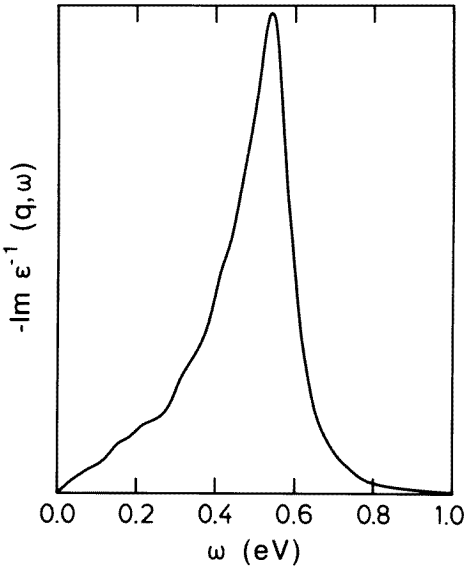

Figure 2. $-\mathrm{Im}\ \epsilon^{-1}(\boldsymbol{q}, \omega)$ for $\boldsymbol{q} = (0.25, 0.0, 0.0)$ in the RPA for a disordered cluster with a large t_{1u} bandwidth (0.8 eV) and a large dielectric function $\epsilon = 25$ due to interband transitions.

For the disordered system, the plasmon energy is generally slightly larger than for the ordered system. For a polycrystalline solid an average over different directions is measured. This leads to an extra broadening if the plasmon energy has a strong dependence on the direction of $\boldsymbol{q}$ relative to the crystal axes. If, however, the plasmon energy is rather independent of the direction of $\boldsymbol{q}$ in the infinite, ordered solid, as is found for the present model [11] and in most other solids, then the calculations suggest that this also remains true for the disordered solid, and the averaging over different directions should not cause a large broadening, in particular for small values of q.

We have also considered if the width could be explained by assuming that the true band width is much larger than that found in band structure calculations, so that a decay in single electron–hole pair excitations would be possible. Thus we have artificially increased the t_{1u} band width to 0.8 eV. We consider $\boldsymbol{q} = (0.25, 0.0, 0.0)$ Å^{-1}. To obtain roughly the experimental plasmon energy, we then had to introduce a background dielectric function $\epsilon = 25$, supposedly describing the effect of interband transitions. We note that the experimental dielectric function is about 4 for $q = 0$ [13], and it is further reduced by about a factor 1.4 to about 2.8 at the $\boldsymbol{q}$ considered [11]. The results are shown in figure 2.

The spectrum shows an asymmetric broadening of about 0.2 eV. Although this broadening is appreciable, it is still substantially smaller than the experimental width. We also note that these results were obtained assuming a larger band width than what is found in band structure calculations and that to obtain the correct plasmon energy we had to use a dielectric function that is probably almost a factor ten too large, although the too-large dielectric function may partly be a problem of the RPA or the model. These considerations therefore make it unlikely that a decay in single electron–hole pairs could explain the width of the plasmon.

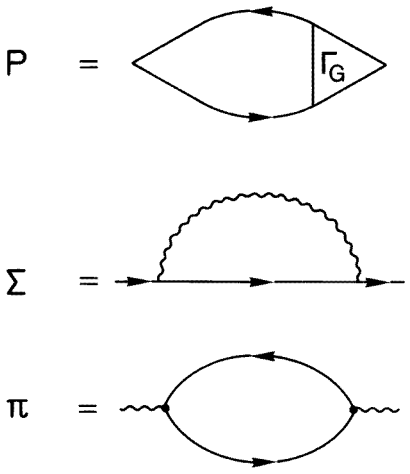

Figure 3. The diagrammatic representation of the irreducible polarization and of the electron and phonon self-energies used here. The electron and phonon Green's functions are represented by solid and curly lines, respectively.The triangle gives the vertex function Γ_G.

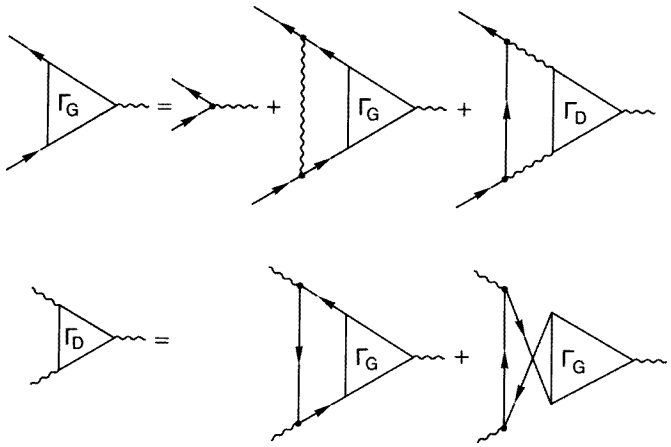

Figure 4. The vertex functions Γ_G and Γ_D. The solid and curly lines show the electron and phonon Green's functions, respectively, and the solid point represents the electron–phonon interaction.

3. Response function with electron–phonon interaction

We express the dielectric function $\epsilon(q)$ in terms of the irreducible polarizability $P(q)$ as

$$\epsilon(q) = 1 - v(q)P(q). \tag{13}$$

where q stands for a $\boldsymbol{q}$ vector and a Matsubara frequency ω_m and $v(q)$ is the Fourier transform of the Coulomb interaction. The polarizability is given by (see figure 3)

$$P(q) = 2\sum_k G(k+q)G(k)\Gamma_G(k,q) \tag{14}$$

where a factor of two comes from the summation over spin, $G(k)$ is the electron Green's function and $\Gamma_G(k,q)$ is a vertex correction. The sum over q stands for

$$\sum_q \equiv \frac{T}{N}\sum_{\boldsymbol{q}}\sum_{\omega_n} \tag{15}$$

where T is the temperature and N is the number of sites in the systems. We here want to focus on the effects of the electron–phonon interaction, and we do not take the Coulomb interaction into account in the calculation of $P(q)$. Thus we express the Green's function G as

$$G(k) = \frac{1}{\mathrm{i}\omega_m - \varepsilon_{\boldsymbol{k}} - \Sigma(k)} \tag{16}$$

where Σ is the electron self-energy in the lowest order in the electron–phonon interaction g

$$\Sigma(k) = -g^2\sum_q G(k-q)D(q). \tag{17}$$

Here $D(q)$ is the phonon Green's function

$$D(q)^{-1} = -\frac{\omega_m^2 + w_0^2}{2\omega_0} - \Pi(q) \tag{18}$$

where ω_0 is the phonon frequency and

$$\Pi(q) = 2g^2\sum_k G(k+q)G(k) \tag{19}$$

is the phonon self-energy to lowest order in the electron–phonon interaction. The self-energies Σ and Π are calculated self-consistently, using dressed Green's functions. A factor of two arises from the summation over spin. These self-energies are shown in figure 3. We now have to construct a vertex function consistent with the electron Green's function. For this purpose we can follow a diagrammatic approach (see figure 4), or following Baym and Kadanoff [14] we can introduce a vertex function $\Gamma_G = -\delta G^{-1}/\delta V$, where V is an external potential. This introduces a second vertex function $\Gamma_D = -\delta D^{-1}/\delta V$. This leads to the following set of equations for the vertex functions

$$\begin{aligned}\Gamma_G(k,q) = 1 &- g^2\sum_{k'} G(k')G(k'+q)D(k-k')\Gamma_G(k',q) \\ &- g^2\sum_{k'} D(k')D(k'+q)G(k-k')\Gamma_D(k',q)\end{aligned} \tag{20}$$

and

$$\begin{aligned}\Gamma_D(k,q) = 2g^2&\sum_{k'} G(k')G(k'+q)G(k'-k)\Gamma_G(k',q) \\ &+ 2g^2\sum_{k'} G(k')G(k'+q)G(k+k'+q)\Gamma_G(k',q).\end{aligned} \tag{21}$$

To show that the vertex function Γ_G satisfies the Ward identity [6], we essentially follow Engelsberg and Schrieffer [15]. We introduce vector vertex functions

$$\begin{aligned}\Gamma_G(k,q) &= \nabla\varepsilon(\boldsymbol{k}) \\ &\quad - g^2\sum_{k'} G(k')G(k'+q)D(k-k')\Gamma_G(k',q) \\ &\quad - g^2\sum_{k'} D(k')D(k'+q)G(k-k')\Gamma_{\boldsymbol{D}}(k',q)\end{aligned} \tag{22}$$

and

$$\begin{aligned}\Gamma_D(k,q) &= 2g^2\sum_{k'} G(k')G(k'+q)G(k'-k)\Gamma_G(k',q) \\ &\quad + 2g^2\sum_{k'} G(k')G(k'+q)G(k+k'+q)\Gamma_G(k',q).\end{aligned} \tag{23}$$

By insertion, we can then check that in the limit $|\boldsymbol{q}| \to 0$ the *ansatz*

$$\mathrm{i}\omega_m\Gamma_G(k,q) - \boldsymbol{q}\cdot\Gamma_G(k,q) = G^{-1}(k+q) - G^{-1}(k) \tag{24}$$

leading to

$$\mathrm{i}\omega_m\Gamma_D(k,q) - \boldsymbol{q}\cdot\Gamma_D(k,q) = 0 \tag{25}$$

satisfies (20)–(23). Since $|\boldsymbol{q}| \to 0$, we obtain the generalized Ward identity

$$\mathrm{i}\omega_m\Gamma_G(k,q) = G^{-1}(k+q) - G^{-1}(k) \tag{26}$$

which follows from charge and current conservation [15]. This relation is also satisfied if we put $\Gamma_D(k,q) \equiv 0$, which leads to a formalism advocated by Engelsberg and Schrieffer [15].

4. Model and details of calculations

We use a one-band model with coupling to local Einstein phonons on each site. These phonons describe the intramolecular H_g phonons in C_{60}, which provide the important electron–phonon coupling in C_{60}. This model neglects that there are eight fivefold degenerate H_g phonons and that the partly occupied t_{1u} band is threefold degenerate, since the purpose of the present calculations is only to study if the phonon mechanism can provide a broadening of the right order of magnitude. We thus consider the Hamiltonian

$$\begin{aligned}H &= \sum_{\boldsymbol{k}\sigma}\varepsilon_{\boldsymbol{k}}n_{\boldsymbol{k}\sigma} + \omega_0\sum_{\boldsymbol{q}}(b_{\boldsymbol{q}}^{\dagger}b_{\boldsymbol{q}}) \\ &\quad + \frac{g}{\sqrt{N}}\sum_{\boldsymbol{k},\boldsymbol{q}\sigma} c_{\boldsymbol{k}+\boldsymbol{q}}^{\dagger}c_{\boldsymbol{k}}(b_{\boldsymbol{q}} + b_{-\boldsymbol{q}}^{\dagger}) \\ &\quad + \frac{v(q)}{N}\sum_{\boldsymbol{k},\boldsymbol{k}'\boldsymbol{q}} c_{\boldsymbol{k}+\boldsymbol{q}}^{\dagger}c_{\boldsymbol{k}'-\boldsymbol{q}}^{\dagger}c_{\boldsymbol{k}'}c_{\boldsymbol{k}}\end{aligned} \tag{27}$$

where $\varepsilon_{\boldsymbol{k}}$ are the energies of the electrons, ω_0 is the energy of the Einstein bosons, g is the electron–phonon coupling and $v(q) = 4\pi e^2/(\Omega\epsilon q^2)$ is the Coulomb interaction, with Ω being the unit cell volume and $\epsilon = 4$ the dielectric constant due to interband transitions. The operators $c_{\boldsymbol{k}}$ and $b_{\boldsymbol{q}}$ are the annihilation operators of the electrons and phonon, respectively. We use an fcc lattice and describe the electrons in a tight-binding

scheme with a nearest-neighbour hopping t_1. We also included a small second-nearest-neighbour hopping t_2 ($t_2/t_1 = -0.4$) to avoid perfect nesting. The electron–phonon coupling constant λ, entering in superconductivity, is given by

$$\lambda = \frac{2g^2 N(0)}{\omega_0} \approx \frac{2g^2}{\omega_0 B} \tag{28}$$

where $N(0)$ is the density of states per spin at the Fermi energy and B is the bandwidth. We use $\omega_0 = 0.2$ eV, which corresponds to the highest H_g mode and $g = 0.2$ eV. Using the band width $B = 0.6$ eV, we obtain $\lambda \approx 0.3$, which corresponds to the coupling to the two highest H_g modes, according to an estimate based on photoemission for a free C_{60}^- molecule [16].

To perform the calculations we consider a large cluster of $16^3 = 4096$ sites. The calculations are performed at a finite temperature of $T = 70$ K, which is smaller than the typical energy scales of the problem. The Green's functions are calculated for 256 Matsubara frequencies, which corresponds to an energy cut off of about 5 eV, i.e., ten times larger than the largest energy scale of the problem, namely the band width. The fast Fourier transform technique is used to transform the various quantities between real space and imaginary times on the one hand and reciprocal space and Matsubara frequencies on the other hand. In this way time consuming calculations of convolutions and correlations can be turned into simple multiplications. For instance, in the first sum in (20) we introduce $F(k') = G(k')\Gamma_G(k', q)G(k' + q)$. The sum can then be written as the simple convolution $\sum_{k'} F(k')D(k - k')$, which is performed by transforming all the quantities to real space and imaginary time, followed by a simple multiplication in this space and a transformation back to the original space. An iterative procedure was used for solving the integral equations (20) and (21). A Padé approximation is used to analytically continue the results to the real-frequency axis [17].

5. Results

In figure 5 we show the experimental results for the electron energy loss function as a function of the energy and momentum transfer for K_3C_{60}. The data are normalized to the intensity of the volume plasmon at about 25 eV. These results were obtained at room temperature by electron energy-loss spectroscopy (EELS) measurements in transmission using a 170 keV spectrometer [18]. The energy and momentum resolution were chosen to be 120 meV and 0.05 Å^{-1}, respectively. Single-phase K_3C_{60} films were grown using vacuum distillation [19, 20]. The film thickness was about 1500 Å. Details of the sample preparation and characterization are given elsewhere [21]. The raw data have been corrected for elastic line contributions. The plasmon peak position is independent of q within the experimental accuracy, implying a very small dispersion of the plasmon, and the width is about 0.5 eV, independently of q and comparable to the plasmon energy. The peak at about 1.3 eV is related to an interband $t_{1u} \rightarrow t_{1g}$ transition. This transition has also been observed in other potassium intercalated C_{60} compounds like K_6C_{60} and K_4C_{60} [22].

In figure 6 we show the electron spectral function for three values of $\boldsymbol{k}$. The spectral function at the L point, which is close to the Fermi energy, shows two structures with a substantial weight at about the phonon energy above and below the main peak, due to phonon satellites. In addition there are tails extending further away from the quasiparticle peak. For the electron at the X point (bottom of the band) spectral weight is pushed outside the lower edge of the bare band and at the Γ point (top of the band) weight is pushed above the top of the bare band. This leads to a large effective band width.

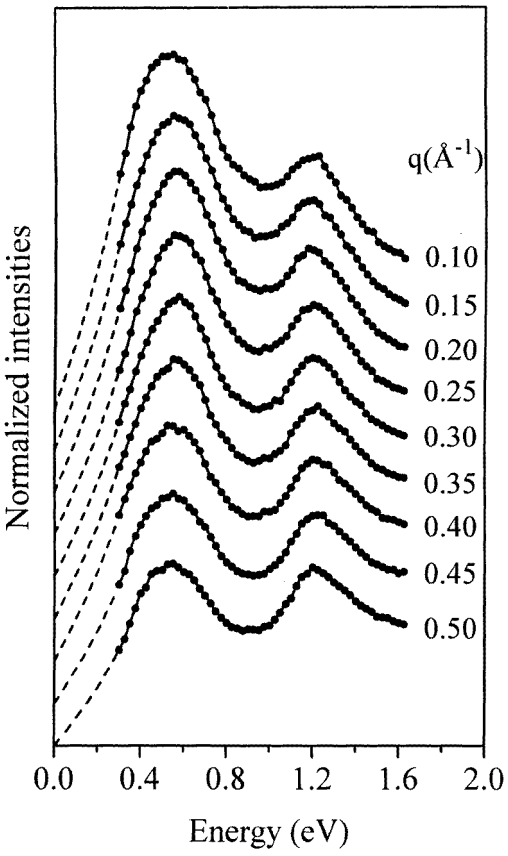

Figure 5. The experimental loss function for K_3C_{60} as a function of energy for different values of the momentum transfer. The dashed line indicates the energy region where the curves have been extrapolated to zero energy after elastic line subtraction.

To understand the electron spectral function better, we first consider the electron self-energy calculated using zeroth-order electron and phonon Green's functions.

$$\Sigma(k,\omega) = g^2 \sum_p \left\{ \frac{1-f(p)}{\omega - \varepsilon_p - \omega_0 + \mathrm{i}\delta} + \frac{f(p)}{\omega - \varepsilon_p + \omega_0 - \mathrm{i}\delta} \right\}. \tag{29}$$

Assuming a band with a constant density of states and width B, we obtain

$$\Sigma(k,\omega) = \frac{1}{2} \left\{ \ln \frac{\omega + B/2 + \omega_0 - \mathrm{i}\delta}{\omega + \omega_0 - \mathrm{i}\delta} + \ln \frac{\omega - \omega_0 + \mathrm{i}\delta}{\omega - B/2 - \omega_0 + \mathrm{i}\delta} \right\}. \tag{30}$$

Figure 7 shows the self-energy in (30) for $\delta = 0.01$ eV. The imaginary part is non-zero for frequencies between ω_0 and $\omega_0 + B/2$. This corresponds to the scattering of an electron into a state with the energy between 0 and $B/2$ and the simultaneous excitation of a phonon. For small frequencies, the self-energy behaves roughly as $\Sigma \sim -\lambda\omega$, as found for a large bandwidth [23]. The negative sign leads to a reduced dispersion of the quasiparticles. For somewhat larger energies of the order $\omega_0 + B/2$, however, the real part of the self-energy is large and positive, due to the finite band-width leading to a zero imaginary part for larger energies. This is completely different from the case $B/2 \gg \omega_0$ where the electronic states

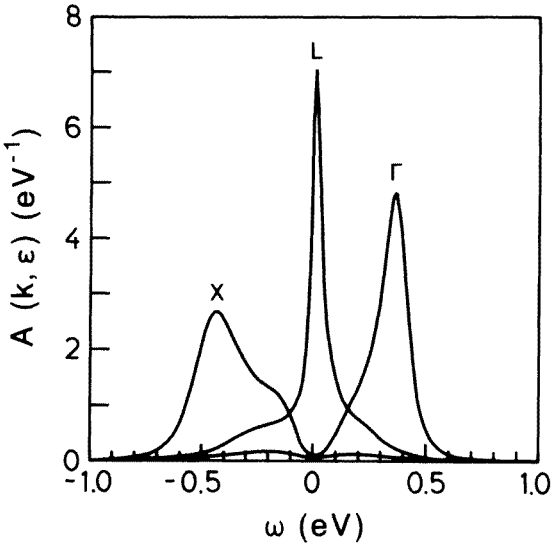

Figure 6. The electron spectral function at the Γ point (0,0,0), the X point $2\pi/a(1, 0, 0)$ and the L point $\pi/a(1, 1, 1)$.

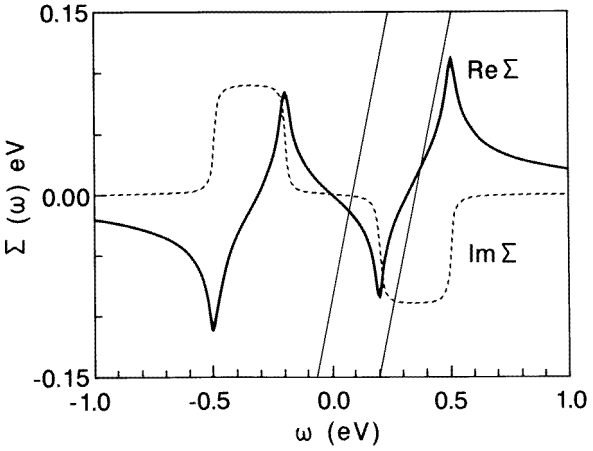

Figure 7. The electron self-energy for a system with a constant density of states and using undressed Green's functions. The two straight lines show $\omega - \varepsilon_k$ for $\varepsilon_k = 0.09$ and 0.35, respectively. The positions of the crossings with $\mathrm{Re}\Sigma(\omega)$ illustrate how the quasiparticles corresponding to $\varepsilon_k = 0.09$ and 0.35 are shifted to lower and higher energies, respectively.

are pushed towards the Fermi energy, while in the present case the quasiparticles close to the band edges of the bare band tend to be pushed out of the band. This explains the spectral functions in figure 6 and the large band width. To support these arguments, we show in figure 8 the calculated self-energy for the Γ point, using the zeroth-order electron and phonon Green's functions as before but with the real band structure, and in figure 9 we show the self-energy using the dressed Green's functions. We can see that figures 8 and 9 are qualitatively similar to figure 7. Similar results for Σ were obtained for the X and

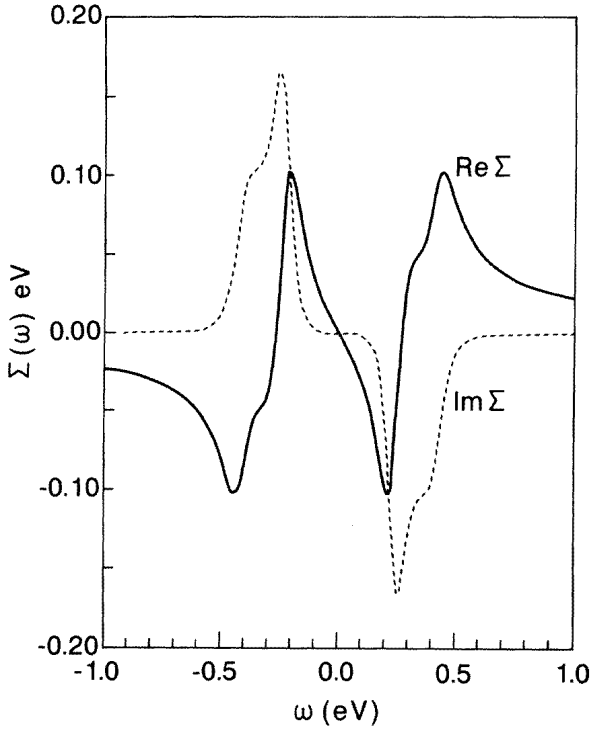

Figure 8. The electron self-energy at the Γ point using undressed Green's functions.

L points. This increase of the quasiparticle band width is important for the damping of the plasmon.

Figure 10 shows the phonon spectral function. The peak is shifted towards lower frequencies by almost a factor of two compared with the zeroth-order spectral function, which is a δ-function at $\omega_0 = 0.2$ eV. The reason for this large shift is that the whole coupling is to one single mode, while in a more realistic model the coupling would be split up over several, fivefold degenerate H_g modes, and the shift would be correspondingly smaller. There is a substantial broadening.

Figure 11 shows $-\mathrm{Im}\,\epsilon^{-1}(\boldsymbol{q}, \omega)$ with the electron–phonon interaction included. We first notice that the peak corresponding to the plasmon has a width of the right order of magnitude (0.4 eV), and that the electron–phonon interaction provides a likely mechanism for the broadening. It is also interesting that neglect of vertex corrections does not substantially change the results. We further note that the vertex correction Γ_D is typically a factor of four smaller than Γ_G.

6. Summary

We have presented electron energy-loss spectra for single-phase K_3C_{60}, showing that the 0.5 eV charge carrier plasmon has a large width ($\sim$ 0.5 eV). An RPA calculation for a supercell with 32 C_{60} molecules shows that the orientational disorder of the C_{60} molecules should not be responsible for this broadening. In particular, the coupling between plasmons for different values of q introduced by the disorder is small. We have performed a calculation

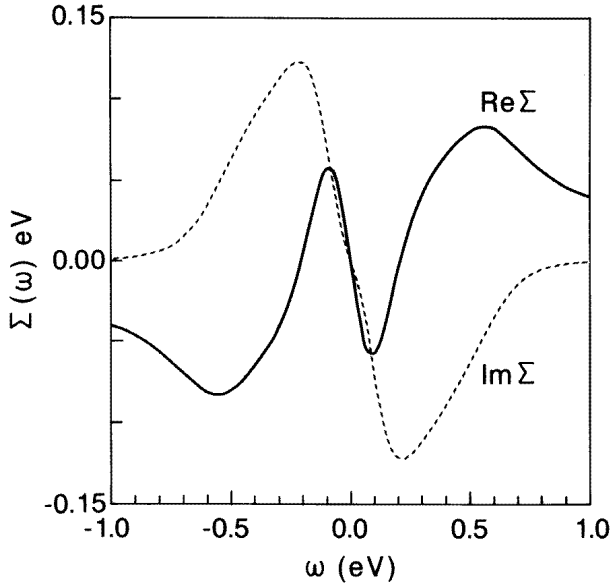

Figure 9. The electron self-energy at the Γ point using dressed Green's functions.

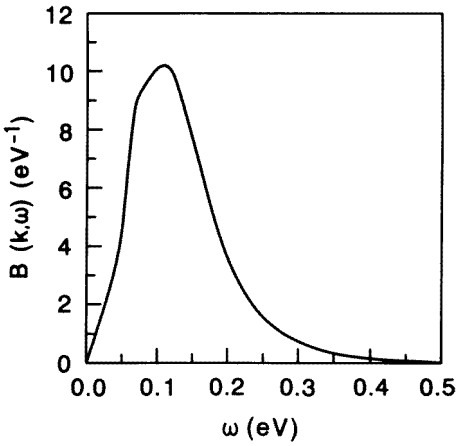

Figure 10. The phonon spectral function for L point $\boldsymbol{q} = \pi/a(1, 1, 1)$. A very small broadening of 0.004 eV (full-width half-maximum) has been introduced.

of the dielectric function including the electron–phonon coupling. The lowest-order electron and phonon self-energy diagrams were calculated self-consistently. The response function was then calculated, including vertex corrections which satisfy the Ward identity. It was found that this leads to a large broadening of the plasmon peak, which is comparable to the observed experimental broadening. The small width of the bare electron band is important for the influence of the electron–phonon coupling on the electronic states. While in the broad band case the electron states are pushed towards the Fermi energy, in the present problem states close to the bare band edges are pushed away from the Fermi energy, increasing the width of the quasiparticle band. This width is therefore about twice the plasmon energy,

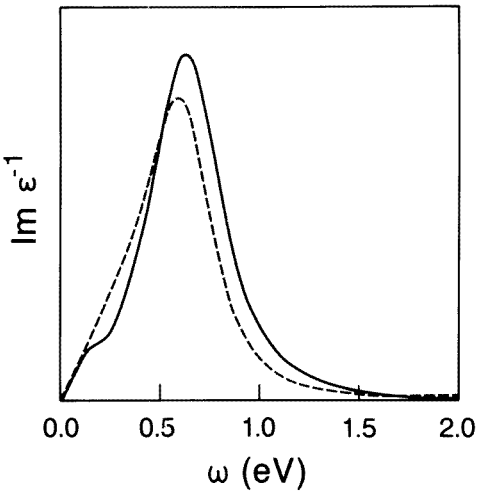

Figure 11. $-\mathrm{Im}\,\epsilon^{-1}(\boldsymbol{q},\omega)$ including the electron–phonon coupling with $\boldsymbol{q} = 2\pi/a(0.25, 0.25, 0.25)$. The full and dashed curves show results with and without vertex corrections, respectively.

and the decay of the plasmons in dressed electron–hole pairs is energetically allowed. We note that the large electron–electron interaction [24, 25, 26] could also contribute to the broadening. It would therefore be interesting to calculate the dielectric function in a similar formalism but with the Coulomb interaction included.

Acknowledgments

We would like to thank L Hedin for interesting discussions. This work has been supported in part by the European Community program Human Capital and Mobility through contract No CHRX-CT93-0337.

References

[1] Sohmen E, Fink J and Krätschmer W 1992 *Europhys. Lett.* **17** 51
[2] Erwin S C and Pickett W E 1991 *Science* **254** 842
Satpathy S, Antropov V P, Andersen O K, Jepsen O, Gunnarsson O and Liechtenstein A I 1992 *Phys. Rev.* B **46** 1773
[3] Antropov V P, Mazin I I, Andersen O K, Liechtenstein A I and Jepsen O 1993 *Phys. Rev.* B **47** 12 373
[4] Stephens P W, Mihaly L, Lee P L, Whetten R L, Huang S-M, Kaner R, Deiderich F and Holczer K 1991 *Nature* **351** 632
[5] Varma C M, Zaanen J and Raghavachari K 1991 *Science* **254** 989
Schluter M, Lannoo M, Needels M, Baraff G A and Tomanek D 1992 *Phys. Rev. Lett.* **68** 526; 1992 *J. Phys. Chem. Solids* **53** 1473
Mazin I I, Rashkeev S N, Antropov V P, Jepsen O, Liechtenstein A I and Andersen O K 1992 *Phys. Rev.* B **45** 5114
Antropov V P, Gunnarsson O and Liechtenstein A I 1993 *Phys. Rev.* B **48** 7551
Mitch M G, Chase M G and Lanny J S 1992 *Phys. Rev. Lett.* **68** 883; 1992 *Phys. Rev.* B **46** 3696
Prassides K, Christides C, Rosseinsky M J, Murphy D W and Haddon R C 1992 *Europhys. Lett.* **19** 629
[6] Ward J C 1950 *Phys. Rev.* **78** 182
[7] Holstein T 1964 *Ann. Phys. (N.Y.)* **29** 410
[8] Gunnarsson O, Satpathy S, Jepsen O and Andersen O K 1991 *Phys. Rev. Lett.* **67** 3002

[9] Mazin I I, Liechtenstein A I, Gunnarsson O, Andersen O K, Antropov and V P Burkov S E 1993 *Phys. Rev. Lett.* **26** 4142
Mazin I I, Liechtenstein A I, Gunnarsson O and Andersen O K 1994 *Solid State Commun.* **91** 497
[10] Teslic S, Egami T and Fischer J E 1995 *Phys. Rev.* B **51** 5973
[11] Gunnarsson O, Eyert V, Knupfer M, Fink J and Armbruster J F 1996 *J. Phys.: Condens. Matter* **8** 2557
[12] Gunnarsson O and Zwicknagl G 1992 *Phys. Rev. Lett.* **69** 957
Gunnarsson O, Rainer D and Zwicknagl G 1992 *Int. J. Mod. Phys.* B **6** 409
[13] Hebard A F, Haddon R C, Flemming R M and Kortan R 1991 *Appl. Phys. Lett.* **59** 2109
[14] Baym G and Kadanoff L P 1961 *Phys. Rev.* **124** 287
Baym G 1962 *Phys. Rev.* **127** 1391
[15] Engelsberg S and Schrieffer J R 1963 *Phys. Rev.* **131** 993
[16] Gunnarsson O, Handshuh H, Bechthold P S, Kessler B, Ganteför G and Eberhardt W 1995 *Phys. Rev. Lett.* **74** 1875
[17] Vidberg H J and Serene J W 1977 *J. Low Temp. Phys.* **29** 179
[18] Fink J 1989 *Adv. Electron Electron Phys.* **75** 121
[19] Poirier D M 1994 *Appl. Phys. Lett.* **64** 1356
[20] Knupfer M, Poirier D M and Weaver J H 1994 *Phys. Rev.* B **49** 8464
[21] Knupfer M, Fink J, Armbruster J F and Romberg H A 1995 *Z. Phys.* B **98** 9
[22] Knupfer M, Armbruster J F, Romberg H A and Fink J 1995 *Synth. Met.* **79** 1321
[23] Grimvall G 1981 *The electron–phonon coupling in metals* (Amsterdam: North-Holland)
[24] Lof R W, van Veenendaal M A, Koopmans B, Jonkman H T and Sawtzky G 1992 *Phys. Rev. Lett.* **68** 3924
[25] Brühwiler P A, Maxwell A J, Nilsson A, Mårtensson N and Gunnarsson O 1993 *Phys. Rev.* B **48** 18 296
[26] Antropov V P, Gunnarsson O and Jepsen O 1992 *Phys. Rev.* B **46** 13 647